

Gamma Ray Pulsars: Emission from Extended Polar Cap Cascades

Joseph K. Daugherty

Department of Computer Science, University of North Carolina at Asheville, Asheville, NC
28804

Alice K. Harding

Laboratory for High Energy Astrophysics, NASA/Goddard Space Flight Center,
Greenbelt, MD 20771

ABSTRACT

Subject headings: gamma rays: theory

1. INTRODUCTION

In recent years the Compton Gamma Ray Observatory (CGRO) and other instruments have provided major new discoveries and detailed observations of isolated γ -ray pulsars, including the Crab (Nolan et al. 1993), Vela (Kanbach et al. 1994), Geminga (Halpern & Holt 1992, Bertsch et al. 1992, Mayer-Hasselwander et al. 1994), PSR B1509-58 (Wilson et al. 1992), PSR B1706-44 (Thompson et al. 1992), PSR B1055-52 (Fierro et al. 1993), and most recently PSR B1951+32 (Ramanamurthy et al. 1995). Models of these objects must now account for a variety of detailed features in the emission, especially from the most intense sources (Crab, Vela, Geminga). Current models have in fact already encountered problems in explaining how these sources can show both remarkable similarities and puzzling variations in their light curves and phase-resolved energy spectra. These difficulties are even more severe if models of the γ -ray emission must also be consistent with the radiation observed at radio, optical, and X-ray wavelengths. As the observational statistics for the weaker sources improve, these theoretical challenges may become even more formidable.

At present two general types of γ -ray pulsar models are popular in the literature. The Polar Cap (PC) model, first proposed by Sturrock (1971) and later investigated by numerous authors (see for example Ruderman and Sutherland 1975, Harding 1981, Daugherty and Harding 1982, Arons 1983) assumes that the emission is produced by electrons accelerated to high energies just above the surface of a magnetized rotating neutron star (NS), in the vicinity of the magnetic poles. In contrast, the Outer Gap model (Cheng, Ho, and Ruderman 1986a, 1986b) places the acceleration regions much higher in the NS magnetosphere, in vacuum gaps formed within a charge-separated plasma.

In a previous paper (Daugherty and Harding 1994, hereafter DH94) we proposed a version of the PC model based on the following principal assumptions:

(a) The gamma emission is initiated by the acceleration of electrons from the NS surface, just above the magnetic PC regions which enclose the *open* magnetic field lines extending to the velocity-of-light cylinder (LC).

(b) The emission originates as curvature radiation (CR) produced by the electrons as they follow the curvature of the open magnetic field lines.

(c) The processes of direct $1 - \gamma$ pair conversion (see for example Erber 1966) by the NS magnetic field and synchrotron radiation (SR) by the emitted pairs produce photon-pair cascades, from which the observed γ radiation emerges.

(d) The rotational and magnetic axes of the radiating NS are nearly aligned, so that the inclination α is small enough to be comparable with the PC half-angle θ_{pc} . More precisely,

the model requires that $\alpha \sim \theta_b$ where θ_b is the half-angle of the γ -beam emerging from the PC.

Assumptions (a)-(c) comprise essentially the original postulates of the PC model (Sturrock 1971). They describe the overall physics of the cascade process and in combination they determine the form of the production spectra for the gamma rays and the pairs. The final assumption (d) primarily affects the viewing geometry. It implies that randomly oriented observers should see emission from at most one PC. However, since CR-induced cascades are intrinsically hollow-cone sources which produce their most intense emission near the PC rim, observers viewing a single PC may detect light curves with either single or double peaks (DH94). Sterner and Dermer (1994) independently noted a similar effect in a model of PC cascades initiated by Comptonization rather than CR. The assumption that $\alpha \sim \theta_b$ allows the phase separation between double peaks to become large enough to match the observed values (~ 0.4 for the Crab and Vela, ~ 0.5 for Geminga).

In the present work we refine assumption (d) by requiring *only* that $\alpha \sim \theta_b$, not that α itself be necessarily small. Hence in place of the Nearly Aligned Rotator (NAR) model described in DH94, we consider here a more general Single Polar Cap (SPC) model. In addition, we introduce a further assumption which allows θ_b (and α) to have significantly larger values than θ_{pc} itself:

(e) the acceleration of the electrons occurs over an extended distance above the PC surface, so that they reach their peak energies at heights of a few NS radii. Above these heights, the acceleration is cut off by an overlying force-free plasma.

In DH94 we neglected the height of the acceleration region and simply supplied the electrons with an injection energy at the NS surface, then traced their CR energy losses as they escaped outward along field lines for which $\mathbf{E} \cdot \mathbf{B} \sim 0$. We have since noted that the assumption of an extended acceleration region provides a solution to a serious difficulty with our previous model, namely the “observability” problem. This refers to the fact that if conventional estimates of PC dimensions are accurate, γ -beams emitted by energetic electrons just above the NS surface would be so small that there would be a low probability ($\lesssim 10^{-2}$) that they could be detected by randomly oriented observers. In our previous work we noted that the usual estimate for the PC radius R_{pc} may in fact be too small, although moderate increases in R_{pc} cannot by themselves resolve the observability problem. However, the outward flaring of the magnetic field lines implies that the half-angle θ_b of the (hollow) cascade γ -beams increases rapidly with height above the NS surface. Thus the effect of extending the acceleration zone up to heights of a few NS radii, especially if combined with moderately increased ($\lesssim 2$) PC dimensions, can produce rotating beams whose edges sweep over a much larger solid angle.

In DH94 we also noted that in order to produce double peaks as narrow as those observed from the Crab, Vela, and Geminga, we had to assume that the surface density of the electrons drawn from the NS surface is concentrated near the PC rim. In the present work we suggest a physical basis for this empirical observation, namely the acceleration of secondary cascade electrons created near the rim. More precisely, the excess rim density may be supplied by a multistep process initiated by the reversed acceleration of secondary positrons created just below the acceleration cutoff height. These particles can produce downward-oriented cascades, creating new pairs near the NS surface. A fraction of the electrons from these pairs may then be accelerated upward along with the true primary electrons, adding to the net outward flow. We argue that this sort of cascade feedback process should occur preferentially near the PC rim, where the open magnetic field lines have their maximum curvature.

2. EXTENDED PAIR CASCADES

In our treatment of the NAR Model in DH94, we assumed that the acceleration of PC electrons starts at the NS surface and is cut off sharply at a height $h \ll R_{pc}$ by an overlying force-free pair plasma. This assumption was made partly for simplicity, and also because there is still no firmly established, self-consistent electrodynamical model for magnetospheric acceleration, either near the NS surface or elsewhere. However, we note that a significant problem with these models may be resolved if the accelerating potential $\Phi(h)$ extends upward to heights $h \sim 2 - 3$ NS radii or higher. We will first discuss our motivation for exploring extended acceleration regions, then describe our model results based on specific empirical choices for $\Phi(h)$.

For simplicity we retain our NAR model assumption that each PC is almost circular with radius $R_{pc} = R_{ns}\theta_{pc}$, where R_{ns} is the NS radius. While the more general SPC model allows larger values of α and hence noncircular PCs, this approximation should be still adequate for our present treatment. For purely dipolar fields, the conventional estimate for the half-angle θ_{pc} is just

$$\sin \theta_{pc} = \left(\frac{R_{ns}}{R_{lc}} \right)^{1/2} = \left(\frac{R_{ns}\Omega}{c} \right)^{1/2} \quad (1)$$

where $R_{lc} = c/\Omega$ denotes the distance to the velocity-of-light cylinder and Ω is the NS angular rotation frequency. Eq. (1) assumes that a dipole field line, emerging from a point near the PC rim, should close just inside the light cylinder. However, as we noted in DH94 this estimate ignores all plasma effects and thus should be regarded only as a lower limit on θ_{pc} . For example, Michel (1982, 1991) has found that the presence of a force-free, rigidly corotating plasma (even without inertial effects or outward current flow) causes a distortion of the field lines which increases the PC radius by a factor ~ 1.3 . Hence we argue that a more realistic model could be expected to increase θ_{pc} by a factor ~ 2 over Eq. (1).

If we make the usual assumption that the magnetic field is purely dipolar, the equation describing a given field line emerging from the PC is just

$$r = k \sin^2 \theta \quad (2)$$

where k is constant. At a given point on the field line, the angle ψ of the local tangent (measured from the magnetic axis) is given by

$$\tan \psi = \frac{3 \sin \theta \cos \theta}{3 \cos^2 \theta - 1} \quad (3)$$

If the gamma beam size is approximately determined by the locus of tangents to the outermost open field lines, for $\theta_{pc} \ll 1$ a cascade gamma beam originating from the NS surface would have a half angle $\theta_b \sim \tan \psi \sim \frac{3}{2}\theta_{pc}$.

In general we can use Eqs. (2) and (3) to estimate the increase in beam width $\theta_b \sim \psi$ with height, for a given PC radius. Figure 1 illustrates this height dependence by plotting the tangent angle ψ vs. radial distance along the field lines, for the case of the Vela pulsar ($P = 0.89$ ms). The curves labeled 1, 2,... denote field lines emerging from the NS surface at the corresponding multiples of θ_{pc} as given by Eq. (1). It is evident that if the cascade gamma emission extends upward to heights exceeding ~ 3 NS radii, $\theta_b \sim \psi$ can become significantly larger than $\frac{3}{2}\theta_{pc}$. This effect is even more pronounced if θ_{pc} is taken to be ~ 2 or more times the standard estimate (1).

3. ACCELERATION AND ENERGY LOSSES ABOVE POLAR CAPS

We have shown that from the standpoint of viewing geometry, extended PC cascades may provide a viable solution to the observability problem. The obvious next step is to examine the possibility that the acceleration of electrons from the PC surface might be sustained up to heights of several NS radii. This question also requires us to consider in detail the energy loss mechanisms which may affect the net acceleration.

Due to the intense ($\sim 10^{12}G$) NS magnetic fields, electrons accelerated from the PC surface are constrained by rapid SR losses to follow the field lines. Hence they obey a one-dimensional equation of motion, which may be expressed as an energy-balance equation:

$$\frac{d\gamma}{ds} = (\beta c)^{-1} \left[\left(\frac{d\gamma}{dt} \right)_{acc} - \left(\frac{d\gamma}{dt} \right)_{cr} - \left(\frac{d\gamma}{dt} \right)_{cs} - \left(\frac{d\gamma}{dt} \right)_{other} \right] \quad (4)$$

Here γ denotes the electron Lorentz factor, $\beta = v/c$, and s is the distance traversed along the field line. The subscripts labeling the component energy gain and loss rates are defined as follows.

The subscript *acc* denotes the energy gain due to electrostatic acceleration in regions where $\mathbf{E} \cdot \mathbf{B}$ is nonzero. We assume this term is proportional to \mathbf{E}_{\parallel} , the component of \mathbf{E} parallel to \mathbf{B} , at each point along the particle trajectory (magnetic field line). Unfortunately, current models of pulsar magnetospheres do not agree on the behavior of $\mathbf{E}_{\parallel}(\mathbf{r})$ near the PC surface. Hence the energy-gain term in Eq. (4) must be regarded as unknown. However, we can at least assume various simple models for the accelerating potential (e.g. Ruderman and Sutherland 1975, Arons 1983) in our simulations and compare the results for each model with observations. In Sections 6 and 7 we show that we have been able to find self-consistent models of extended cascades which yield light curves and spectra similar to the observed

values. We have also identified significant constraints on the accelerating field which are critical to the viability of these models.

In contrast to the gain-rate term, the principal loss-rate terms in Eq. (4) are reasonably well understood. The subscripts *cr*, *cs*, and *other* denote energy losses due to CR, Compton upscattering (Dermer 1990, Chang 1995), and other scattering processes respectively. One example of the latter is triplet pair production (Mastichiadis et al. 1986, Mastichiadis 1991, Dermer and Schlickeiser 1991). Sturmer (1995) has recently provided a systematic treatment of PC electron acceleration which considers these energy-loss processes in detail. We have used his expressions for the CS loss terms in our simulations, although his treatment involves a number of simplifying approximations.

The CR loss rate has the simple form (see for example Jackson 1975)

$$\left(\frac{d\gamma}{dt}\right)_{cr} = \frac{2}{3} \frac{e^2}{mc} \frac{\gamma^4}{\rho_c^2} \quad (5)$$

where ρ_c is the local radius of curvature of the magnetic field line. For a purely dipolar field, the exact expression for ρ_c is just

$$\rho_c = \frac{k(\sin^4 \theta + \sin^2 2\theta)}{\sin^4 \theta + 2 \sin^2 2\theta - 2 \sin^2 \theta \cos 2\theta} \quad (6)$$

Since Eq. (6) yields values $\sim 10^7$ cm for standard PC model parameters, the CR loss rate only becomes significant for $\gamma \gtrsim 10^6$. At higher energies it is by far the dominant loss mechanism.

The CS loss rate results from upscattering of ambient photons by the accelerated electron beam. In our model the photon background consists of thermal emission from the NS surface, and hence the CS loss rate should only be significant only at heights $h \lesssim R_{ns}$ above the surface. Pulsed X-ray observations of Geminga (Halpern and Ruderman 1993) and PSR B1055-52 (Ögelman and Finley 1993) suggest that for at least some sources the thermal background may include multiple components at distinct temperatures (e.g., emission from both the cooling NS surface and hotter regions in the vicinity of the PCs).

The CS loss rate is found from the general expression (Dermer 1990, Sturmer 1995)

$$\left(\frac{d\gamma}{dt}\right)_{cs} = c \int d\epsilon \int d\Omega n_{ph}(\epsilon, \Omega) (1 - \beta \cos \Psi) \int d\epsilon'_s \int d\Omega'_s \frac{d\sigma'}{d\epsilon'_s d\Omega'_s} (\epsilon_s - \epsilon) \quad (7)$$

where $\epsilon = \hbar\omega/m_e c^2$ is the incident photon energy in units of the electron rest energy, $n_{ph}(\epsilon, \Omega)$ is the number density of incident background photons within energy and solid-angle increments $d\epsilon$ and $d\Omega$, and Ψ denotes the angle between these photons and the local electron

beam direction. The quantity $d\sigma'/d\epsilon'_s d\Omega'_s$ is the magnetic Compton scattering cross section in the local electron rest frame (ERF), where the primes denote quantities evaluated in the ERF and the subscript s labels scattered photon quantities.

In the strong magnetic field the CS cross section includes both nonresonant and resonant components (Herold 1979, Daugherty and Harding 1986, Bussard et al. 1986). Dermer (1990) has derived a nonrelativistic approximation for the loss rate based on the magnetic Thomson cross section in the ERF (Herold 1979), resolving the total loss rate into component terms which he labels ‘angular’, ‘nonresonant’, and ‘resonant’. Sturmer (1995) has applied further simplifying assumptions to these terms in order to derive convenient expressions for the CS loss rate. His results are summarized in his equations (4)-(9), which we have incorporated into our acceleration tracing algorithm.

Sturmer (1995) notes that for $\gamma \gtrsim 10^3$, the incident thermal photon energies above the cyclotron resonance may become relativistic ($\epsilon' \gtrsim 1$). In this case he replaces the nonresonant component of the cross section by a relativistic (but nonmagnetic) Klein-Nishina expression given by his equations (10)-(14). In this work we have included these expressions, although we note that a more accurate treatment will require the use of the magnetized (resonant) Klein-Nishina cross section (Daugherty and Harding 1986, Bussard et al. 1986).

The only loss term which Sturmer (1995) includes under the ‘other’ label in Eq. (4) arises from electron-photon scattering events in which the scattered photon is replaced by an emergent e^+/e^- pair. Using cross sections found by Mastichiadis et al. (1986) and Mastichiadis (1991) for the nonmagnetic form of this process, Sturmer (1995) applies a monoenergetic photon approximation to derive a loss rate given by his equation (16). For our model parameters this term is never dominant, but for generality we have also included it in our simulation. As in the case of his Klein-Nishina CS loss rate, however, we note that in future work the magnetic form of this process should be investigated since it may also exhibit resonant behavior which may increase its significance.

4. SIMULATIONS OF EXTENDED PC CASCADES

The basic features of our cascade simulation code are described in DH94. The version used in this work includes several major improvements. These include revised adaptive algorithms for tracing photon propagation, which allow more accurate localization of near-threshold pair conversion events. We have also improved the tracing of synchrotron/cyclotron emission, which now more accurately simulates both recoil and angular distribution effects in the cyclotron regime ($\gamma \gtrsim 1$).

However, the most significant improvement for this work is the algorithm for tracing electron acceleration through extended regions above the PC. In our current version, each primary electron emerges from the surface with an initial Lorentz factor $\gamma_0 \gtrsim 1$. Assuming specific parameters for both the energy gain and loss mechanisms as described in Section 3 above, the calculation then traces the net acceleration of the electron as it escapes outward along the local magnetic field line. For this purpose we have developed an adaptive numerical technique to integrate Eq. (4) which accomodates a wide range of energies and distance scales. To estimate the significance of Compton losses due to thermal photons from the NS surface we have used a model similar to that employed by Sturmer (1995), in which the PC has a uniform surface temperature T_6 (in units of $10^6 K$) within a circle of radius R_{tpc} centered on each magnetic pole. This region is defined as the *thermal* PC. Note that R_{tpc} may differ from the PC radius as defined by the locus of the outermost open field lines. In fact we treat both T_6 and R_{tpc} as parameters in the model. At present we ignore any softer emission which may be emitted from the overall surface.

Figure 2 shows sample acceleration profiles $\gamma(h)$, where h is the height above the NS surface in stellar radius units. Curve (a) shows a case in which the accelerating field is assumed to be constant, namely $(d\gamma/ds)_{acc} = 5 \text{ cm}^{-1}$, from the surface up to a sharp cutoff at height $h_c = 3$. Curves (b) and (c) both assume that the gain rate is a linearly increasing function $(d\gamma/ds)_{acc} = 5h$, over this same region. They differ only in the assumed values for the Comptonization parameters, namely the thermal PC temperature T_6 and radius R_{tpc} (measured in NS radius units). Curve (b) assumes $T_6 = 1$ and $R_{tpc} = 0.1$, corresponding to a cool, small thermal PC. The opposite case of a hot, large PC, is shown by curve (c) which assumes $T_6 = 2$ and $R_{tpc} = 0.5$. We note that the constant-acceleration curve (a) is not affected by these variations of the Comptonization parameters, since in this case the gain rate greatly exceeds the loss terms in Eq. (4). We also observe that even the linear-acceleration profiles are sensitive to the Comptonization parameters only for heights $h \ll 1$, and they have little effect on the peak energies reached at the cutoff height h_c .

As γ exceeds values $\gtrsim 10^6$ the primary CR emission reaches gamma ray energies, re-

sulting in photon-pair cascades. The calculation, as described in DH94, recursively traces the full cascade development and accumulates 3D tables of emergent γ -ray counts vs. energy and solid angle, from which we derive spectra and light curves of the emission as seen from arbitrary viewing directions. In this work we have accumulated photon counts from ensembles of primary electrons distributed in concentric rings over the PC surface. We have assumed that the primary beam current is axisymmetric with respect to the magnetic axis, hence the electrons in each ring are spaced uniformly in azimuth. However, our analysis facility allows us to assign arbitrary weights to the γ counts from each ring. This technique allows us to vary the assumed radial dependence of the primary electron current density without requiring new runs of the simulation.

Finally we should point out that our current simulation is based strictly on a CR-initiated cascade, i.e. it considers Comptonization as an energy loss mechanism acting on the primary electrons but it does not yet include the upscattered photons as a source of high-energy γ -rays which may themselves initiate cascades. This is in obvious contrast to the cascade model proposed by Sturmer and Dermer (1994), in which Comptonization provides *all* the high-energy input photons. Under our model assumptions the primaries reach much higher peak energies ($\gamma \gtrsim 10^6$) than the values they assume ($\gamma \sim 10^5$), so that in our case CR should initiate the bulk of the cascade emission. However, we recognize that Comptonization may add a measurable contribution to the emergent γ -emission and in a separate work we will extend the cascade simulation to trace the CS upscattered photons as well. At the same time, we note that the CS contribution may be expected to produce a narrower γ -beam than the extended CR component we consider here, since it should originate closer to the PC surface. Thus it is possible that PC cascades initiated by CR and CS photons may be distinguishable both spatially and energetically.

5. ELECTRON CURRENTS NEAR THE PC RIM

In DH94 we showed that single magnetic poles can exhibit doubly peaked light curves with phase separations $\delta\phi \lesssim 0.5$ if $\alpha \sim \theta_b$ and the observer angle $\zeta \sim \alpha$. However, in order to reproduce the small duty cycles of the double peaks seen in the Crab, Vela, and Geminga, we had to impose an additional *ad hoc* assumption that the primary electron density is strongly concentrated near the PC rim. We also noted that there are two possibilities for obtaining doubly peaked profiles with $\delta\phi < 0.5$, in which the designations of *leading* and *trailing* peaks are reversed. In DH94 we considered in detail the case in which the first peak corresponds to the phase at which the observer viewpoint emerges from the interior of the (hollow) γ -beam, while the second peak marks the point of reentry. This case, which we denote as the Exterior Scenario (ES), can produce $\delta\phi < 0.5$ if the rotational axis is contained within the γ -beam ($\alpha < \theta_b$). By combining the ES with the assumption that the primary current is concentrated near the PC rim, we could account for both the short duty cycles and the lack of emission outside the peaks (since this would be the phase interval during which the observer viewpoint penetrates the interior of the hollow beam). In this scenario we associated the finite emission observed between the peaks with residual, higher-altitude cascades, which would produce emission with larger beam widths.

In work following DH94 we have compared our model predictions in detail with CGRO observations of phase-resolved spectra for the Vela pulsar (Kanbach et al. 1994). We have concluded that the ES does not provide uniformly consistent fits to the spectra, especially for the phase intervals between the main peaks. In the ES model the high-altitude cascades which produce the interpeak emission do tend to produce harder spectra below their characteristic high-energy turnovers, since a smaller fraction of the hard CR emission is converted to softer cascade photons. By itself this trend is at least qualitatively consistent with the observations. However, the peak CR energy ($\propto \gamma^3$) also decreases rapidly as the primaries lose energy above the acceleration zone, with the result that the turnovers in the interpeak cascade spectra drop to lower energies compared to the peak spectra. In this respect the model prediction is opposite to the observed trend.

This problem with the ES has led us to reexamine the alternative labeling of the leading and trailing peaks, in which the PC interior is identified as the source of the interpeak emission. We refer to this case as the Interior Scenario (IS). In order to produce finite interpeak emission in this case, we must abandon the phenomenological DH94 model of a pure rim distribution for the primary electrons. However, if we replace the pure rim model with a two-component model which includes a uniform interior current, it turns out that the IS allows a more consistent overall agreement with the observations than the ES. Moreover, in this scenario we can suggest a tentative physical interpretation for a two-component

primary current. In particular, the uniform component is a simple approximation of a Goldreich-Julian (GJ) current $I_{GJ} = \pi R_{pc}^2 c \rho_0$ (Goldreich and Julian 1969), where

$$\rho_0 \sim \frac{-\mathbf{\Omega} \cdot \mathbf{B}}{2\pi c} \quad (8)$$

which should be valid if $\theta_{pc} \ll 1$. We propose that this component includes all the true *primary* electrons drawn from the NS surface. In this view the extra rim component consists of secondary electrons from pairs preferentially created near the PC rim, where the increasing field-line curvature produces more rapid γ -pair conversions.

If any secondary pairs contribute to the PC current of high-energy particles which initiates cascades, the pairs must themselves be accelerated to energies comparable with the peak primary energies. This in turn would require at least some pairs to be created well below the acceleration cutoff height. If (as we assume here) the primaries are negative electrons (e^-), each e^- secondary would then move *upward* and thus add to the GJ primary current, while the e^+ would be accelerated *downward* along the local field line toward the surface. In fact the model γ -ray light curves we present in Section 6 show that if just a small fraction ($\sim 10^{-2}$ or less) of the cascade pairs created near the rim can be boosted to $\gamma \gtrsim 10^6$, a two-component current model shows good agreement with observations.

In spite of these results, we must first consider a fundamental theoretical objection to the acceleration of secondary pairs. The problem is that the onset of cascade pair production is expected to produce a sharp cutoff in the acceleration of the primaries at a height h_c , which marks the boundary of the overlying pair plasma (e.g. Ruderman and Sutherland 1975, Arons 1983). Our own simulation results confirm that the quenching of E_{\parallel} above h_c should be an abrupt process, since the density of created pairs is found to rise sharply with height. This is demonstrated in Figure 3, which plots typical growth curves of the multiplicity $M = (N_s^+ + N_s^-)/N_p$ where N_p and N_s denote the numbers of primaries and secondaries respectively. Thus even if pairs created at the lowest heights can be accelerated by a decreasing E_{\parallel} within a finite transition zone, the growth curves indicate that this zone is too short for any e^- secondaries to reach energies comparable to those of the primaries. This appears to eliminate the most obvious model for enhancing the PC current near the rim, in which the negative pair members are accelerated outward with the primaries.

However, the positron (e^+) component in such a transition zone must also be subject to acceleration. The key point here is that these particles may be drawn *downward* from the transition zone back into the acceleration zone, following the local field lines back toward the NS surface. In fact they should traverse a distance comparable to the full extent of the acceleration zone, and thus reach energies sufficient to create (tertiary) pairs by a variety of possible mechanisms (e.g. $\gamma - B$ pair production, triplet pair production). The result

would be the creation of pairs deep within the acceleration zone, whose e^- members could be accelerated outward with the primaries to reach similar peak energies.

This sort of cascade feedback process should be most likely to occur above those regions of the PC where the original upward-directed cascades initiated by the primaries commence at the lowest heights. Unless the electrostatic acceleration varies greatly over the PC interior regions, the increasing curvature of the field lines from the pole to the rim implies that the primary cascades develop first near the rim (cf. Figure 3). Hence we argue that reverse e^+ -acceleration and downward-oriented cascades occur preferentially around the rim.

As a first test of this hypothesis we have generalized our acceleration tracing algorithm to follow secondary positrons downward from creation points just below the cutoff height, back toward the NS surface. The results confirm that these particles can be boosted to $\gamma \lesssim 10^7$ at heights $h \gtrsim R_{ns}$ above the surface, allowing their CR spectra to reach pair-conversion energies and initiate downward-oriented cascades. In a separate work we will refine our complete simulation code to investigate the development of these cascades in detail. We anticipate that their presence may impact our model in several respects, since in addition to providing a new source of electrons these cascades can influence the behavior of the acceleration process just above the surface. In particular, if the cascades create a sufficiently dense layer of pair plasma overlying the surface they can retard acceleration below the effective height of this layer. In addition, it is possible that energetic downstreaming cascade photons can impose severe Comptonization losses on upward-directed electrons. As described in the following sections, in this work we will allow for these possibilities by considering simple models in which the acceleration may effectively commence at finite heights above the NS surface.

6. GAMMA-RAY LIGHT CURVES

The 3D photon count tables accumulated by the simulation may be summed over energy bins to produce 2D sky maps of the γ -emission between arbitrary energy limits. An example is shown in Figure 4, which plots a grayscale contour map of emission over 100 MeV. Any horizontal line drawn across this plot corresponds to a specific value of the polar angle ζ for a given viewing direction, and the counts distributed along this line define the γ -ray light curve as seen from this viewpoint.

Following the arguments in Section 5 we present sample results for the Vela pulsar using a simple two-component primary current model, which we obtain by superimposing simulation datasets for concentric rings of primaries as discussed in Section 4. In each case we

have included a total of 10 rings spaced at equal radial increments to cover the PC interior. Since each ring contains 180 particles with a uniform 2-degree azimuthal spacing, the inner rings are weighted $\propto r^{-1}$ to approximate a uniform interior density. To simulate test cases with a moderate rim component, we have weighted the outermost ring by arbitrary factors in the range 3 to 5. Physically this corresponds to the acceleration of a few secondary electrons for each primary electron on this ring, which is a small fraction of the $10^2 - 10^3$ cascade pairs created per primary near the rim.

All the datasets we have accumulated to date assume the following general form for the accelerating field, namely

$$E_{\parallel}(h) = \frac{mc^2}{e} \left(\frac{d\gamma}{ds} \right)_{acc} = \frac{mc^2}{e} [a_0 + a_1(h - h_0)] \Theta(h - h_0) \Theta(h_c - h) \quad (9)$$

We choose units for Eq. (9) such that the path length s is measured in cm, while the height $h = (R - R_{ns})/R_{ns}$ is in NS radius units from the PC surface, $\Theta(x)$ is the unit step function (0 for $x < 0$, 1 for $x > 0$), and the constants a_0 , a_1 , and h_0 are taken as free parameters in our model. Their values effectively determine the height at which cascades commence above the PC rim, which Arons (1983) denotes as the “pair formation front”. In the following we take the height at which the cascade multiplicity exceeds unity (cf. Figure 3) as a reasonable measure of the acceleration cutoff height h_c . Thus h_c is a function of (a_0, a_1, h_0) but is *not* itself a free parameter. In practice we determine h_c from trial simulations before generating complete datasets.

The quantity $h_0 \geq 0$ in Eq. (9) denotes the height at which acceleration commences. We introduce h_0 to allow for the possibility that downward-oriented cascades may prevent or impede acceleration just above the NS surface. As noted in Section 5, this can occur either if the cascades create a sufficiently dense layer of pair plasma overlying the surface, or if downstreaming cascade photons impose strong Comptonization losses on upward-moving electrons. In a separate study of downward-oriented cascades we will investigate both of these effects in order to put physical constraints on the choice of h_0 , but here we simply explore the effects of varying h_0 in sample models.

If we let $a_1 = 0$ in Eq. (9) we obtain a constant-field approximation, resembling vacuum gap acceleration models of the type proposed by Ruderman and Sutherland (1975). If instead we set $a_0 = 0$, we have a crude approximation for the potential suggested by Arons (1983) in his slot-gap model. We have generated datasets for the Vela pulsar using both of these limiting forms. In each case we have empirically chosen combinations of the parameters (a_0, a_1, h_0) such that the primary electrons reach their peak energies ($\gamma \gtrsim 10^6$) rapidly enough to initiate cascades. We note that in this work we have assumed no dependence of either a_0 , a_1 , or h_0 on the magnetic polar angle θ . We have used a further simplifying assumption

here, namely that the cutoff height h_c has the same value over the PC interior as determined by the onset of cascades near the rim. While this assumption must be questioned in a more refined treatment, we show below that it leads to encouraging agreement with observations.

Figure 5(a,b,c,d) shows model light curves obtained under these assumptions for the acceleration function Eq. (9), using sample parameters $(a_0, a_1, h_0) = (5, 0, 0)$, $(0, 5, 0)$, $(0, 20, 1)$, and $(50, 0, 2)$, which we denote as models A, B, C, and D respectively. Table 1 lists additional simulation parameters which are common to all these models. In models A-C a common weight factor of 5 was assigned to the outermost ring of primary electrons to represent the excess rim current, while a factor 3 was used for model D. (The simulation would assign a weight factor of 1 to this ring for a uniform distribution.) In each case the rim weights were chosen to obtain reasonable fits to the observed Vela light curve. Since each simulation includes a total of 10 concentric primary current rings covering the PC interior, these rim weight factors increase the total PC currents above their uniform component values by factors of roughly 1.7 for models A-C and 1.4 for model D. For comparison, in each of these plots the light curves which would be produced by the uniform current alone (without the excess rim component) are shown in gray.

If we compare these model results with the observed Vela light curve (Kanbach et. al 1994) shown in Figure 9, we see that the acceleration parameters which best match the observations are those for which the acceleration near the surface is low. In fact, satisfactory fits are obtained only if the primaries do not reach $\gamma \gtrsim 10^6$ until after they have attained heights $h \gtrsim 1$. If they exceed these energies at altitudes too far below the cutoff height h_c , the total cascade emission which they produce over the full acceleration region and beyond is spread over large solid angles, yielding broad pulse peaks. In particular, this tendency rules out constant-acceleration models ($a_1 = 0$) such as that shown in Figure 5(a), except in cases where $h_0 \gtrsim 2$ as in Figure 5(d). A comparison of Figures 5(b), 5(c) shows that even for linear acceleration ($a_0 = 0$), the fits are significantly improved by introducing nonzero values of h_0 .

Among the sample runs shown in Figure 5, models C and D show peak duty cycles which are in the best agreement with the observed values. Moreover, in each of these cases the first half of the interpeak emission resembles both the magnitude and slope seen in the data. This example shows that the two-component model for the primary current can produce consistent agreement with a significant portion of the total light curve. Unfortunately the agreement breaks down for the trailing interpeak component, but since our model assumes axisymmetric current rings it cannot account for any strong asymmetry in the light curve.

Finally we note that all these models predict a low but finite level of emission throughout the phase interval between Peak 2 and Peak 1 (i.e., over regions outside the PC rim). This

emission is due to the residual, high-altitude cascades which we suggested in DH94 might be the source of the interpeak emission. Kanbach et al. (1994) find no detectable emission in this phase interval for Vela, and no evidence for unpulsed emission. Given their stated estimates for the EGRET detector sensitivity, however, their findings are not in conflict with our model results for the sample datasets C and D described above. However, the observations do impose an additional constraint on the relative weight factors for the two-component PC current distribution. For example a uniform PC current, without any rim current enhancement, would produce significantly more emission outside the peaks than the observations allow.

7. PHASE-RESOLVED ENERGY SPECTRA

The same choices of parameters (model C and D) which best match the observed light curves in Section 6 also produce the best fits for the energy spectra. In spite of the similar appearance of their light curves, however, model D produces better spectral fits than model C. In fact, as shown in Figure 6 model D provides the closest match to the observed total (phase-averaged) spectrum across five decades in energy. The spectral differences among these models are principally due to their varying extent of cascade development. In models A and B the primary electrons reach maximum energies of 7.5×10^6 and 1.2×10^7 respectively, compared to 1.7×10^7 for Model C and 2.0×10^7 for Model D. The values for models A and B especially are too low to supply either the photons up to 3 GeV or the level of emission observed below 100 MeV. Clearly, the observed Vela total emission is not the result of curvature radiation alone.

Figure 7 shows that this agreement for model D applies not only to the total spectra, but also to the phase-resolved spectra observed by EGRET (Kanbach et. al. 1994). These plots show fits for various phase intervals defined by these authors in their power law-fits to the Vela phase-resolved spectra for energies between 70 and 4000 MeV. The normalization factors were determined separately at each phase interval to match the data and differ by less than a factor of 2. We note that the model reproduces the tendency for the (quasi) power-law spectra at the phase intervals of the two peaks to become significantly softer than the spectra for the interpeak subintervals. In the Interior Scenario (Section 5) this trend is expected since the interpeak emission is due to the interior primary electron current, whose hard CR emission is less efficiently converted to softer cascade photons (cf. Figure 3). The IS model also reproduces the observational feature that the high-energy turnovers in the Vela spectra occur at lower energies for the peaks vs. the interpeaks. The sharpness of

the high-energy turnovers in the P1 and P2 spectral intervals, due to magnetic one-photon pair production attenuation, are also reproduced, especially in P1. The model D spectra in the phase intervals LW1 and TW2, the emission just outside the peaks, turnover more gradually and at energies below 500 MeV. This emission is primarily curvature radiation at high altitudes from primary electrons that have lost a significant amount of their maximum energy. These phase intervals are thus predicted to have the softest spectra, consistent with both the data and the high indices of the power law fits of Kanbach et al. (1994). In model D, the hard spectra in intervals I1 and I2 extend to energies below 10 MeV, predicting that the interpeak emission should decrease relative to that of the peak emission at lower energies. This appears to be verified by the 0.07 - 0.6 MeV light curves measured by OSSE (Strickman et al. 1995), where no interpeak emission was detected.

One quantitative measure of the spectral evolution during each pulse is the hardness ratio H , defined here as the ratio of the flux over 300 MeV to the flux between 100 and 300 MeV. Figure 8 shows the model D hardness ratio vs. pulse phase for $\zeta = 16^\circ$, corresponding to the phase-resolved spectra in Figure 7. The trend toward harder spectra during the interpeak phase interval is clear and appears to be consistent with EGRET Vela observations (Fierro et al. 1995).

8. TOTAL GAMMA FLUX ESTIMATES

If we identify the uniform component of our model PC current with the GJ current predicted by Eq. (8), we can estimate an upper limit on the absolute γ -ray flux levels expected from our model sources within any specified energy range ΔE_γ . The required inputs are the dataset sky map counts, the pulse period P , and the estimated distance D (which we take to be 500 pc for Vela). We outline the procedure briefly as follows.

First we derive the effective number of primaries traced in the simulation, taking into account the weight factors assigned to each concentric ring of electrons. Following the arguments in Section 5, we resolve this total number of primaries into two components representing uniform and rim distributions respectively. As noted above, our total flux estimate (uniform plus rim components) assumes that the uniform component is a GJ current. For the flux estimate, the quantity of interest is the number of GJ primaries in the simulation.

After summing the full 3D photon arrays over the energy range ΔE_γ to produce the appropriate 2D sky maps, we find the number ΔN_γ of photons accumulated along a 1-bin strip of constant ζ and angular width $d\zeta$ during one full pulse ($\Delta\phi = 2\pi$). The phase-averaged γ -ray flux F_γ per primary electron at the distance D is then given by

$$F_\gamma = \Delta N_\gamma / 2\pi \sin \zeta d\zeta P D^2 N_{GJ} \quad (10)$$

where N_{GJ} denotes the effective number of GJ primaries in the dataset (excluding the excess rim component). Finally we obtain an absolute total flux estimate by multiplying Eq. (10) by the (maximal) current of GJ primaries from the PC surface as given by Eq. (8).

The predicted fluxes for our Vela models A,B,C,D at energies > 100 MeV as found from this procedure are 7.3×10^{-5} , 1.6×10^{-4} , 2.8×10^{-4} , 2.8×10^{-4} photons $\text{cm}^{-2}\text{s}^{-1}$ respectively. It turns out that these values are all an order of magnitude higher than the average flux observed by EGRET (Kanbach et al. 1994), namely $(7.8 \pm 1.0) \times 10^{-6}$ photons $\text{cm}^{-2}\text{s}^{-1}$ for $E_\gamma > 100$ MeV. Our high model flux levels, which obviously are due to strong beaming factors of the hollow-cone emission, are not by themselves a problem for our model since the GJ estimate should properly be regarded only as an upper limit on the PC current. We note, however, that the model flux estimate does fall closer to the GJ limit as the γ -beam half-angle θ_b is increased. In this respect the excess predicted flux shows that even larger PC dimensions and/or acceleration cutoff heights can be allowed within the framework of the model.

9. COMPARISON WITH OBSERVATIONS AT OTHER WAVELENGTHS

In the preceding sections we have applied the SPC model specifically to the Vela pulsar, in part because both the γ -ray light curves and phase-resolved spectra for this object have been observed in considerable detail. However, our model results for Vela can also account in general terms for the γ -ray emission from other pulsars with doubly-peaked profiles such as the Crab, Geminga, and PSR B1951+32 (Ramanamurthy et al. 1995). The second general class of light curves predicted by the SPC model, namely those with only a single broad peak, may describe PSR B1055-52 (but see below). At present the only source whose γ -ray light curve may be difficult to accommodate is PSR B1706-44 (Thompson et al. 1992), since recent EGRET observations (Thompson et al. 1995) suggest that this object may have a triply-peaked pulse.

However, we must consider whether the SPC γ -ray model is also compatible with observations of pulsed emission at other wavelengths from Vela and the other known γ -ray pulsars. Our primary concern here involves the possible implications of these observations regarding the viewing geometry for each source. In this context we focus especially on three γ -ray pulsars for which we also have strong evidence of thermal X-ray emission from the NS surface, namely Vela itself (Ögelman et al. 1993), Geminga (Halpern and Holt 1993), and PSR B1055-52 (Ögelman and Finley 1993). These objects are of particular interest since the modulation and phase behavior of the X-ray emission should be directly related to the magnetic field geometry at the NS surface. To facilitate the discussion of these sources, in Figure 9 we have assembled their light curves at various wavelengths using a common phase origin for each source. It turns out that each object presents a distinct set of challenges for our model, which we analyze separately below.

Although it shows no evidence of surface thermal X-ray emission we must also consider observations at other wavelengths from the Crab pulsar. The Crab has the distinction of having doubly peaked light curves in phase at all observed wavelengths. However, its optical emission exhibits polarization swings which cause special problems for the SPC model. An additional challenge is presented by recent HST and ROSAT imaging of the inner Crab nebula, which strongly suggest an observer angle $\zeta \lesssim 60^\circ$ (Hester et al. 1995).

(a) Vela (PSR B0833-45)

As shown in Figure 9(a), the pulsed radio emission from Vela (see for example Manchester and Taylor 1977) exhibits a single narrow peak which leads the first γ -ray peak by ~ 0.12 in phase (Kanbach et al. 1994). The radio pulse shows a high degree of linear polarization with an unusually wide swing ($\gtrsim 90^\circ$) in the polarization angle ψ across the pulse. This behavior has been interpreted (Radhakrishnan and Cooke 1969, see also Michel 1991) in terms of the rotating projection of a dipolar magnetic field in the plane orthogonal to the viewing direction. In this model ψ is given as a function of α , ζ , and the pulse phase angle

ϕ by

$$\tan \psi = \sin \alpha \sin \phi / (\sin \zeta \cos \alpha - \cos \zeta \sin \alpha \cos \phi) \quad (11)$$

Several authors (e.g. Lyne and Manchester 1988, Rankin 1990) have attempted to invert this relation to determine the values of α and ζ for various pulsars, although the results to date are subject to controversy (Michel 1991, Miller and Hamilton 1993). However, Eq. (11) does imply that the maximum rate of the polarization swing $R \equiv |d(\tan \psi)/d(\sin \phi)|$ occurs at the phase corresponding to the closest approach of the magnetic axis to the observer direction, which we denote by ϕ_M . If this model is correct, the rapid, extended swing for Vela ($R \sim 5.9$) indicates that the observer viewpoint approaches a magnetic pole to within a few degrees.

As may be seen from Figure 10, the values of α and ζ used in the Vela model datasets discussed in Sections 6 and 7 do not produce polarization swings which are either as rapid or extended as the observed values. However, the real challenge in accounting for the radio pulse in our model is not simply to find better combinations of these parameters. The key point is that if the radio pulse does indeed mark the phase of closest approach to either of the magnetic poles, in the case of Vela its location relative to the γ -ray peaks is inconsistent with the SPC model. In particular, the Interior Scenario requires ϕ_M to lie midway between the two γ peaks, whereas in the Exterior Scenario it is displaced from the midpoint by 0.5 in phase. In contrast, Kanbach et al. (1994) find the phases of the γ peaks (relative to the phase of the radio peak, $\phi_0 = 0$) to be $\phi_{p1} = 0.12$ and $\phi_{p2} = 0.54$ respectively. Hence the standard PC model of the radio pulse asserts that $\phi_M = \phi_0 = 0$, while the IS predicts $\phi_M = (\phi_{p1} + \phi_{p2})/2 = 0.33$ and the ES has $\phi_M = 0.83$. Thus the standard model of the Vela radio pulse is inconsistent with the SPC γ -ray model.

On the other hand, it turns out that both the optical and X-ray light curves for Vela fit much more naturally within the geometry of the IS. As shown in Figure 9(a), the optical emission (Wallace et al. 1977) has a doubly peaked light curve with a smaller peak-to-peak phase separation (~ 0.2) than that seen in the γ -ray regime. Moreover, the γ -ray peaks enclose the optical peaks in the sense that the leading optical peak follows the leading γ peak, while the opposite occurs for the trailing peaks (see for example Manchester and Taylor 1977). In the IS, this sort of optical/ γ phase relationship would hold if the optical and γ emission were beamed in coaxial hollow cones from the PC, with beam angles $\theta_b^{opt} < \theta_b^\gamma$. This in turn suggests that the optical emission might either be associated with interior PC currents, or that it might be produced by the rim current at lower heights than the γ -emission.

Figure 9(a) also shows the pulsed X-ray emission from Vela detected by the ROSAT satellite (Ögelman et al. 1993), which consists of a broad pulse trailing the radio peak, with

the bulk of the emission occurring between the two γ -ray peaks. The harmonic content of the pulse suggests a complex nonsinusoidal structure, although the available X-ray data do not show firm correlations with the optical or γ peaks (or clear evidence of more than one peak). The statistics are unfortunately limited by the fact that the emission contains contributions from the compact nebula as well as the pulsar, and the pulsed fraction of the latter is only about 11%. Ögelman et al. (1993) obtain their best fit to the pulsed component with a soft blackbody spectrum ($T_6 \sim 1.5 - 1.6$). They also note that the total point source (pulsed plus unpulsed) can either be fit with a blackbody spectrum at a similar temperature or with a steep power law ($\Gamma \sim -3.3$), compared to a harder power law ($\Gamma \sim 2.0$) which fits the surrounding compact nebula. Ögelman et al. (1993) suggest that if the pulsed component is actually thermal emission, the modulation may be due either to a nonuniform surface temperature distribution or to anisotropic radiation transfer effects in the magnetosphere. In either case the key point for our model is that the pulsed X-ray emission should then be concentrated near the phase ϕ_M of closest approach of the observer direction to a magnetic pole (Page 1995). To the extent that the bulk of the emission does occur between the γ peaks, the Vela X-ray light curve appears compatible with the IS γ -ray model.

In summary it appears that the observed optical, X-ray, and γ -ray light curves for Vela all seem mutually consistent with the IS, whereas the radio polarization swing cannot have the usual interpretation based on Eq. (11) in either the IS or the ES. At present we have no satisfactory way to account for the phase of the Vela radio pulse within the general framework of any SPC model, unless we invoke the possibility of nondipolar magnetic fields near the NS surface.

However, we should point out that this incompatibility is not simply a problem for our γ -ray model. The same conflict already exists between the standard radio model and the entire class of thermal X-ray models (e.g. Page 1995) in which the peak(s) in the pulsed emission coincide with the closest approach of the magnetic pole(s) to the observer viewpoint.

(b) Geminga (PSR B0630+178)

Although Geminga has long been known to be a strong γ -ray source (Kniffen et al. 1975), it was first discovered to be a pulsar from X-ray observations (Halpern and Holt 1992). Shortly thereafter γ -ray pulses were detected at the X-ray period (Bertsch et al. 1992). To date no pulsed emission has been found at either radio or optical wavelengths, although an optical counterpart has been identified (Bignami et al. 1993).

While the lack of optical and radio light curves prevent the sort of phase comparisons we can make for other sources, both the X-ray and γ -ray data are relatively rich in detail. Figure 9(b) shows the light curves for Geminga at both hard and soft X-ray energies from

ROSAT observations (Halpern and Ruderman 1993) as well as in the EGRET γ -ray regime (Mayer-Hasselwander et al. 1994, Ramanamurthy 1995). As in the case of Vela, the γ -ray light curve above 100 MeV exhibits a two-peak structure with significant interpeak (bridge) emission. The peaks have duty cycles only moderately larger than in Vela, with a phase separation of 0.5. In contrast, Halpern and Ruderman (1993) find that the X-ray light curves at both soft (0.07-0.53 keV) and hard (0.53-1.50 keV) energies consist of broad single pulses. The hard component is somewhat narrower, but perhaps most remarkably the soft and hard components are $\sim 105^\circ$ out of phase.

Halpern and Ruderman (1993) have fit the hard and soft components of the pulsed X-ray spectrum to two blackbody sources at temperatures $T_6 \sim 0.5$ and ~ 3 respectively. These authors suggest that the soft emission is from the overall NS surface, while the hard component arises from hotter regions around a PC. However, they also note that within the available statistics a power-law fit for the harder component is nearly as good as the blackbody fit, which leaves open the possibility of magnetospheric emission mechanisms. In any event the hot PC model of the hard X-ray emission appears to be consistent with the SPC γ -ray model, as in the case of Vela, since as seen in Figure 9(b) the bulk of the hard X-ray pulse from Geminga also lies between the double γ -ray peaks (Halpern and Ruderman 1993).

Unfortunately the modulation of the soft X-ray component and its phase shift relative to the hard component complicate this model. In fact the hard and soft components may not be consistently explained within the framework of *any* NS heating/cooling models which assume dipolar magnetic-field symmetry. This point has led Halpern and Ruderman (1993) to suggest an off-axis dipole model in the case of Geminga.

(c) PSR B1055-52

This source has been detected by EGRET at energies above 300 MeV (Fierro et al. 1993). Figure 9(c) shows that in contrast to the doubly peaked radio pulse, the γ -ray light curve appears to exhibit a single broad peak. However, the available statistics are insufficient to rule out a multi-peaked substructure. The limited data makes it difficult to analyze the phase relationship between the radio and γ pulses, although it may be significant that the precursor of the main radio pulse appears just at the trailing end of the γ peak. It is noteworthy that the radio profile has some similarity to that of the Crab, including a peak-to-peak phase separation $\gtrsim 0.4$ which would require an off-axis dipole in an orthogonal rotator model.

PSR 1055-52 has the distinction of exhibiting the hardest phase-averaged γ -spectrum of all the γ -ray pulsars known to date, with a photon spectrum index of ~ 1.2 . It is worth

noting here that PC cascades can definitely exhibit such hard spectra, although they tend to do so only when both the electron CR losses and pair-conversion rates are comparatively low. These conditions are most likely to apply in specific regions of the magnetosphere, especially close to the magnetic axes and/or at heights of several NS radii above the surface. However, both more detailed γ -ray observations and further modeling of this source will be required to determine how the hardness of the spectrum may constrain the SPC model.

Pulsed X-rays have also been detected from PSR B1055-52 by ROSAT (Ögelman and Finley 1993). As in the case of Geminga, the emission exhibits distinct hard and soft components above and below ~ 0.5 keV, both of which exhibit broad single pulses. Figure 9(c) shows the phase relationships between the X-ray light curves and the pulses at radio and γ -ray energies. As in the γ -ray regime, evidence for substructure in either X-ray component is limited by the available statistics. Another striking similarity with Geminga is the large relative phase shift between the hard and soft X-ray peaks, with the hard component in this case leading by $\sim 120^\circ$. Ögelman and Finley (1993) obtain satisfactory spectral fits using two-component blackbody models, although they find that the hard component may also be fit by a power law which extrapolates up to flux levels in the γ -ray regime comparable with the EGRET observations.

If PSR B1055-52 does in fact have only one γ -ray peak, then its relationship to the X-ray emission may be difficult to explain within the SPC model. The key problem is that the model identifies the phase of a single γ peak with the phase ϕ_M of closest approach of the PC. However, if the hard X-ray component is due to PC heating as proposed for Geminga (Halpern and Ruderman 1993), the X-ray peak indicates a value for ϕ_M in apparent conflict with the γ -ray location. While this difficulty does not arise if the hard X-rays have a magnetospheric origin as Ögelman and Finley (1993) suggest, their phase shift relative to the γ -ray pulse is still problematical.

As in the case of Geminga, however, the modulation of the soft X-ray component and its phase shift relative to the hard component complicate the picture. The fact that the radio pulse for PSR B1055-52 has two peaks, with noteworthy similarities to the Crab radio profile, is also puzzling. However, the principal question regarding the viability of the SPC model for this source is whether the γ -ray light curve is singly peaked. Hopefully further analysis of EGRET data will be able to resolve this question.

(d) The Crab Pulsar (PSR B0531+21)

In contrast to all other γ -ray pulsars, the light curve of the Crab exhibits a doubly peaked structure at all wavelengths observed to date, with the peaks appearing at essentially the same phase positions throughout the entire spectrum. In purely geometric terms

this phase synchronization seems to suggest that a variety of emission processes, which may occur in distinct magnetospheric regions of other pulsars, are spatially coincident in the Crab. In the context of SPC γ -ray models it appears to motivate a search for radio, optical, and X-ray emission mechanisms involving the cascade pairs.

Unfortunately, this approach leads to at least one serious difficulty for the SPC model, namely the optical polarization swings found to occur across each peak (Smith et al. 1988). If both the optical and γ peaks do originate from the same PC rim regions, then the optical swings cannot be due to the sort of rotational projection effect described by Eq. (11) since the extent of the swing through the phase intervals containing each γ -peak cannot exceed a few degrees (cf. Figure 10). However, SPC models for the Crab appear to be compatible in this respect with the radio pulses, which do not exhibit significant polarization swings.

In addition to this problem, a significant constraint on SPC models of the Crab pulsar is posed by recent HST and ROSAT observations of the inner nebula (Hester et al. 1995). These observations appear to confirm numerous earlier suggestions that the observer angle ζ for the Crab is considerably larger ($\lesssim 60^\circ$) than the values ($\sim 15^\circ$) used in our sample Vela datasets. However, this finding does not by itself rule out the SPC model for the Crab, since it turns out that such large values of ζ can be accommodated if we allow the PC dimensions to be $\sim 4 - 5$ times larger than the standard estimate Eq. (1), as opposed to the factor 2 used in our model datasets for Vela. Somewhat smaller values are also adequate if the cascades are assumed to extend up to heights $\gtrsim 3$ NS radii. Thus in the case of the Crab especially, the dimensions of the PC are critical to our model.

10. DISCUSSION

The model we have presented here has at least one significant advantage over an alternative SPC model (Sturmer and Dermer 1994, Sturmer et al. 1995) in which PC cascades are initiated by Comptonization of primaries by soft photons from the NS surface rather than CR emission. As we have shown, extended primary acceleration can easily generate CR-induced cascades at heights reaching up to several NS radii. In contrast, cascades due to Comptonization should be confined to significantly lower regions unless some mechanism for strong beaming of the soft photons is invoked. Assuming that similar PC dimensions are used in both models, the Comptonization model has a more limited ability to overcome the observability problem.

The best results we have obtained to date from the extended cascade SPC model are for those cases in which the net electron acceleration becomes significant only at heights $h \gtrsim R_{ns}$ above the NS surface. However, we have shown in Section 3 that neither resonant Compton scattering of thermal photons from the NS surface nor other known energy loss processes considered in previous PC models can effectively counteract accelerating potentials of the types we have considered over distances of this order. This applies in particular to resonant Compton scattering, even if we assume the highest plausible values for both the surface temperatures and thermal PC radii. Thus it is obviously important to investigate the possibility noted in Section 5, namely that downward-oriented cascades initiated by reversed secondary acceleration can prevent or impede acceleration just above the surface. An obvious next step in the exploration of the SPC model is to trace the development of downward-oriented cascades in detail, and if possible to estimate both their significance as a source of energetic Comptonizing photons and the depth of the surface plasma layer which they may create.

The discussion in Section 9 shows that the phase relationships between light curves at different wavelengths are in fact quite complex. The problem of accounting for all these observations in a self-consistent manner may eventually force us to consider models with asymmetric magnetic field geometries. One initial step in this direction would be to consider off-axis dipolar models of the type suggested by Halpern and Ruderman (1993) in more detail. In such models we anticipate that the modulation of thermal X-ray emission from, say, the PC surface may be significantly out of phase with magnetospheric emission produced above the surface and directed along the open field lines.

11. ACKNOWLEDGEMENTS

We are indebted to Joe Fierro, Gottfried Kanbach, Peter Michelson, P.V. Ramana-murthy, and David Thompson for valuable discussions regarding EGRET observations, and to Mark Strickman for information regarding OSSE and COMPTEL results. We also thank Hakki Ögelman and John Finley for discussions on the pulsed X-ray emission from Vela. Michal Marko provided valuable assistance in the development of our visualization and analysis software. We gratefully acknowledge support for this work from NASA CGRO Guest Investigator Grants for Phases 3 and 4 (JKD, AKH), and from the NASA Astrophysics Theory Program (AKH).

REFERENCES

- Arons, J. 1983, ApJ 266, 215.
- Bertsch, D.L. et al. 1992, Nature, 357, 306.
- Bignami, G.F. et al. 1993, Nature, 361, 704.
- Bussard, R.W. et al. 1986, Phys. Rev. D, 34, 440.
- Chang, H.-K. 1995, A&A, in press.
- Cheng, K.S., Ho, C., & Ruderman, M.A. 1986a, ApJ 300, 500.
- Cheng, K.S., Ho, C., & Ruderman, M.A. 1986b, ApJ 300, 522.
- Daugherty, J.K. & Harding, A.K. 1982, ApJ 252, 337.
- Daugherty, J.K. & Harding, A.K. 1983, ApJ 273, 761.
- Daugherty, J.K. & Harding, A.K. 1986, ApJ 309, 362.
- Daugherty, J.K. & Harding, A.K. 1994, ApJ 429, 325.
- Dermer, C.D. 1990, ApJ 360, 197.
- Dermer, C.D. & Schlickeiser, R. 1991, A&A 252, 414.
- Dermer, C.D. & Sturmer, S.J. 1994, ApJ 420, L75.
- Erber, T. 1966, Rev. Mod. Phys. 38, 626.
- Fierro, J.M. et al. 1993, ApJ, 413, L27.
- Fierro, J.M. et al. 1995, in preparation.
- Goldreich, P. & Julian, W.H. 1969, ApJ, 157, 869.
- Halpern, J.P. & Holt, S.S. 1992, Nature 357, 222.
- Halpern, J.P. & Ruderman, M. 1993, ApJ, 415, 286.
- Harding, A.K. 1981, ApJ 245, 267.
- Harding, A.K. & Daugherty, J. K. 1992, in *Isolated Pulsars*, ed. K. A. Van Riper & C. Ho (Cambridge Univ. Press), p. 279.
- Harding, A.K. & Preece, R.D. 1987, ApJ 319, 939.
- Hester, J.J. et al. 1995, ApJ, in press.
- Jackson, J.D. 1975, *Classical Electrodynamics*, Wiley, New York.
- Kanbach, G. 1990, EGRET Science Symposium, NASA Conf. Pub. 3071.
- Kanbach, G. et al. 1994, A&A, 289, 855.

- Kniffen, D.A. et al. 1975, Proc. 14th Internat. Cosmic Ray Conf. 1, 100 (MPE, Munich, Germany)
- Lyne, A.G, and Manchester, R.N. 1988, MNRAS, 234, 477.
- Manchester, R.N., and Taylor, J.H. 1977, Pulsars, W.H. Freeman, San Francisco.
- Mastichiadis, A. 1991, MNRAS, 253, 235.
- Mastichiadis, A., Marscher, A.P., and Brecher, K. 1986, ApJ 300, 178.
- Mayer-Hasselwander et al. 1994, ApJ 421, 276.
- Michel, F.C. 1982, Rev. Mod. Phys. 54, 1.
- Michel, F.C. 1991, Theory of Neutron Star Magnetospheres, Univ. Chicago Press.
- Miller, M.C, and Hamilton, R.J. 1993, ApJ 411, 298.
- Nolan, P.L. et al, 1993, ApJ 409, 697.
- Ögelman, H. & Finley, J.P. 1993, ApJ 413, L31.
- Ögelman, H. et al. 1993, Nature, 361, 136.
- Page, D. 1995, ApJ 442, 273.
- Radhakrishnan, V., and Cooke, D.J. 1969, Astrophys. Lett. 3, 225.
- Ramanamurthy, P.V. et al. 1995, ApJ Letters, in press.
- Ramanamurthy, P.V. 1995, private communication.
- Rankin, J.M. 1990, ApJ 352, 247.
- Ruderman, M.A. & Sutherland, P.G. 1975, ApJ 196, 51.
- Smith, F.G. et al. 1988, MNRAS 233, 305.
- Strickman, M. 1995, ApJ, submitted.
- Sturmer, S.J. & Dermer, C.D. 1994, ApJ 420, L79.
- Sturmer, S.J. 1995, ApJ, submitted.
- Sturmer, S.J. et al. 1995, ApJ, in press.
- Sturrock, P.A. 1971, ApJ 164, 529.
- Thompson, D.J. et al. 1992, Nature, 359, 615.
- Thompson, D.J. et al. 1995, in preparation.
- Wallace, P.T. et al. 1977, Nature, 266, 692.
- Wilson, R.B. et al. 1992, IAU Circ. No. 5429.

TABLE 1: Cascade Vela Model Parameters

| | |
|--------------------------------|---|
| Period | $P = 89 \text{ ms}$ |
| Surface Magnetic Field | $B = 3 \times 10^{12} \text{ Gauss}$ |
| Inclination | $\alpha = 10^\circ$ |
| NS Radius | $R_{ns} = 10^6 \text{ cm}$ |
| PC Radius | $R_{pc} = 2R_{ns} \sin^{-1} (R_{ns}\Omega/c)^{1/2}$ |
| PC Surface Temperature | $T_{pc} = 2 \times 10^6 \text{ K}$ |
| Thermal PC Radius | $R_{tpc} = 0.5R_{ns}$ |
| Initial Primary Lorentz Factor | $\gamma_0 = 1.0$ |

Acceleration parameters (a_0, a_1, h_0) :

| | |
|----------|--------------|
| Model A: | $(5, 0, 0)$ |
| Model B: | $(0, 5, 0)$ |
| Model C: | $(0, 20, 1)$ |
| Model D: | $(50, 0, 2)$ |

FIGURE CAPTIONS

Fig. 1.— Angle ψ between magnetic axis and tangent to fixed dipole field line $r = k \sin^2 \theta$, as function of radial distance r from NS center. Curves labeled 1, 2, ... correspond to field lines originating from NS surface at polar angles $\theta_{pc}, 2\theta_{pc}, \dots$, where θ_{pc} is PC half-angle estimated by Eq. (1).

Fig. 2.— Lorentz factor γ vs. height h in NS radius units, measured from NS surface. Curve (a) assumes constant-field acceleration model $(d\gamma/ds)_{acc} = 5$ for $0 < h < 3$, while (b) and (c) both assume linear form $(d\gamma/ds)_{acc} = 5h$ over same region for distinct combinations of Comptonization parameters. (b) $T_6 = 1$, $R_{tpc} = 0.1$; (c) $T_6 = 2$, $R_{tpc} = 0.5$.

Fig. 3.— Multiplicity M (number of secondary electrons produced per primary electron) vs. radial distance from NS center. Separate growth curves are shown for each primary electron ring in sample Vela dataset defined in Table 1. These plots assume that $E_{\parallel} \propto a_1 h$ for $h > 0$, where a_1 is independent of magnetic colatitude θ over the PC). However, acceleration is assumed to cut off abruptly above height h_c at which first pairs appear, which is a decreasing function of θ .

Fig. 4.— Angular intensity distribution of gamma emission above 100 MeV, plotted using a linear 10-level grayscale.

Fig. 5.— (a,b,c,d) Simulated Vela γ -ray light curves for emission above 100 MeV, using Model A,B,C,D parameters respectively (see Table 1). Corresponding light curves due to uniform PC currents alone (neglecting rim components) are shown in gray. In each case, observer angle ζ has been chosen to produce peak-to-peak phase separations closest to observed value of 0.424. $\zeta = 12^\circ$ for Model A, 15° for Models B and C, 16° for Model D.

Fig. 6.— (a,b,c,d) Total pulsed energy spectra, $E^2 dN/dE$, for Vela Models A,B,C,D and same observer angles ζ as in Figure 5. Solid lines show emergent cascade gamma emission, while dashed lines show pure CR emission (ignoring magnetic pair production and cascade formation). Data points show observations by EGRET (Kanbach et al. 1994) as well as COMPTEL and OSSE (Strickman et al. 1995).

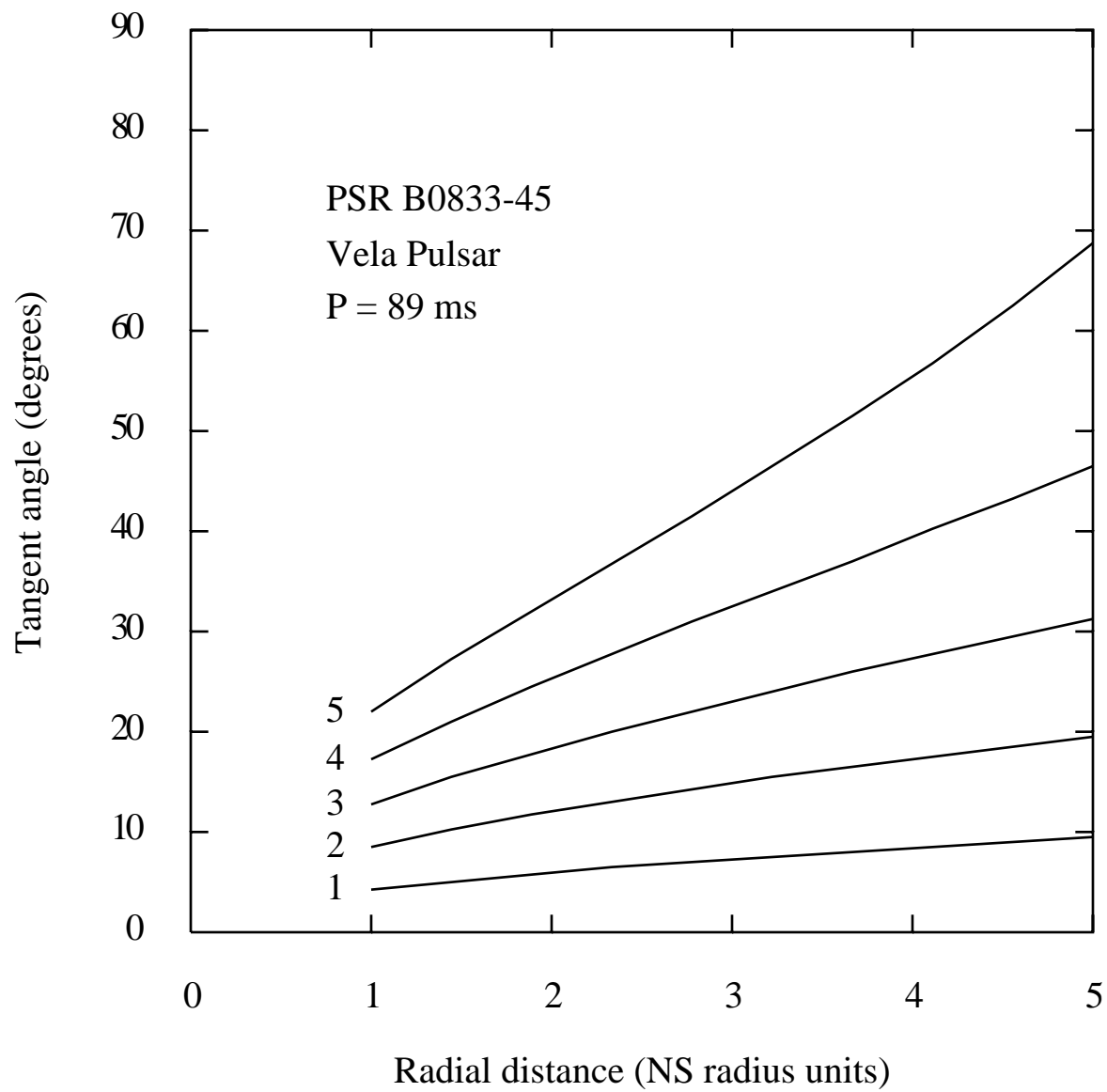
Fig. 7.— Vela Model D phase-resolved spectra, $E^2 dN/dE$, for observer angle $\zeta = 16^\circ$ and phase intervals used in analysis of EGRET data (Kanbach et al. 1994). Solid line shows cascade γ emission, while dashed line shows pure CR emission.

Fig. 8.— Phase-resolved hardness ratios for Vela Model D, assuming $\zeta = 16^\circ$ as in Figure 7.

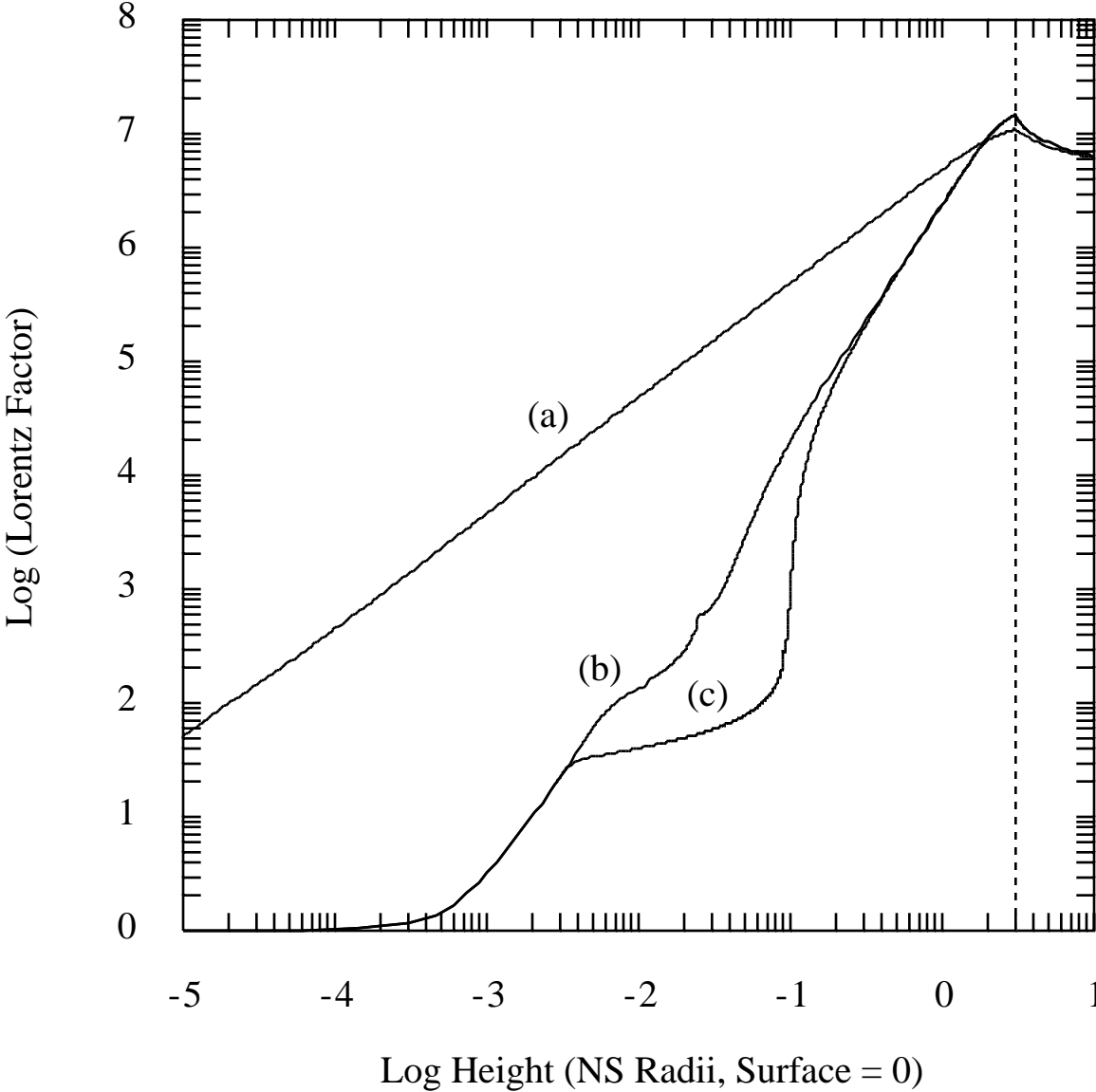
Fig. 9.— Relative phases of X-ray and γ -ray pulses for γ -ray pulsars which appear to emit thermal X-ray emission from the NS surface. Where applicable, emission at radio and optical wavelengths is also shown. (a) Vela; (b) Geminga; (c) PSR B1055-52.

Fig. 10.— Swing of radio linear polarization angle ψ predicted by Eq. (11) for parameters $\alpha = 10^\circ$, $\zeta = 16^\circ$. Dashed lines show phase intervals containing γ -ray peaks in light curves for these models. Maximum predicted slope of polarization curve for these choices of (α, ζ) is $|R| \sim 1.7$, compared to observed value of ~ 6.5 . Discrepancy in slope indicates that actual observer viewpoint has closer approach to magnetic pole than model values (α, ζ) allow. Phase location of radio peak poses more serious problem, since dipolar versions of both SPC γ -ray model and thermal surface emission models of pulsed X-ray emission suggest that phase of closest PC approach is incompatible with standard PC model of radio polarization swing.

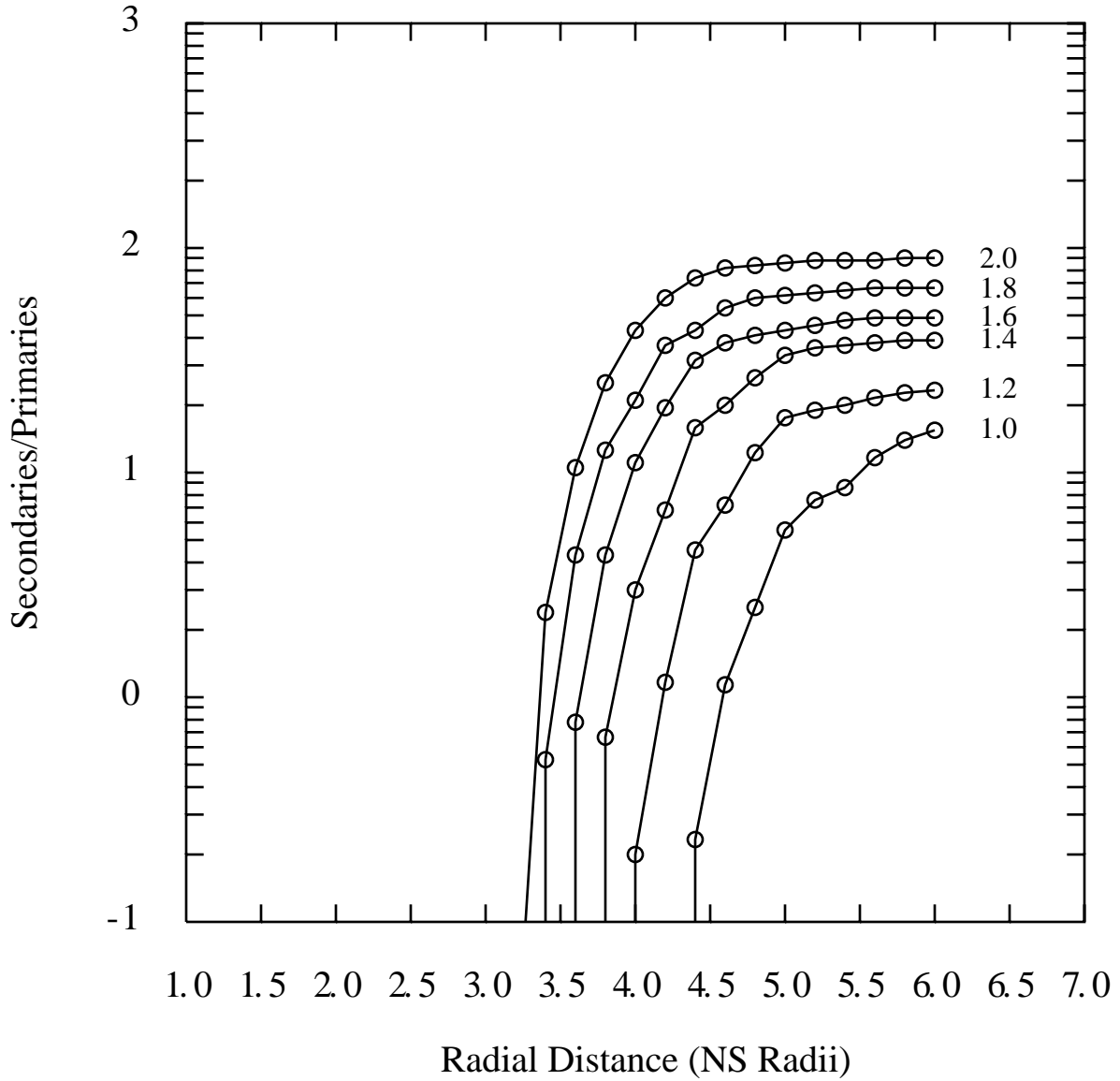
Field Line Tangent vs. Radial Distance



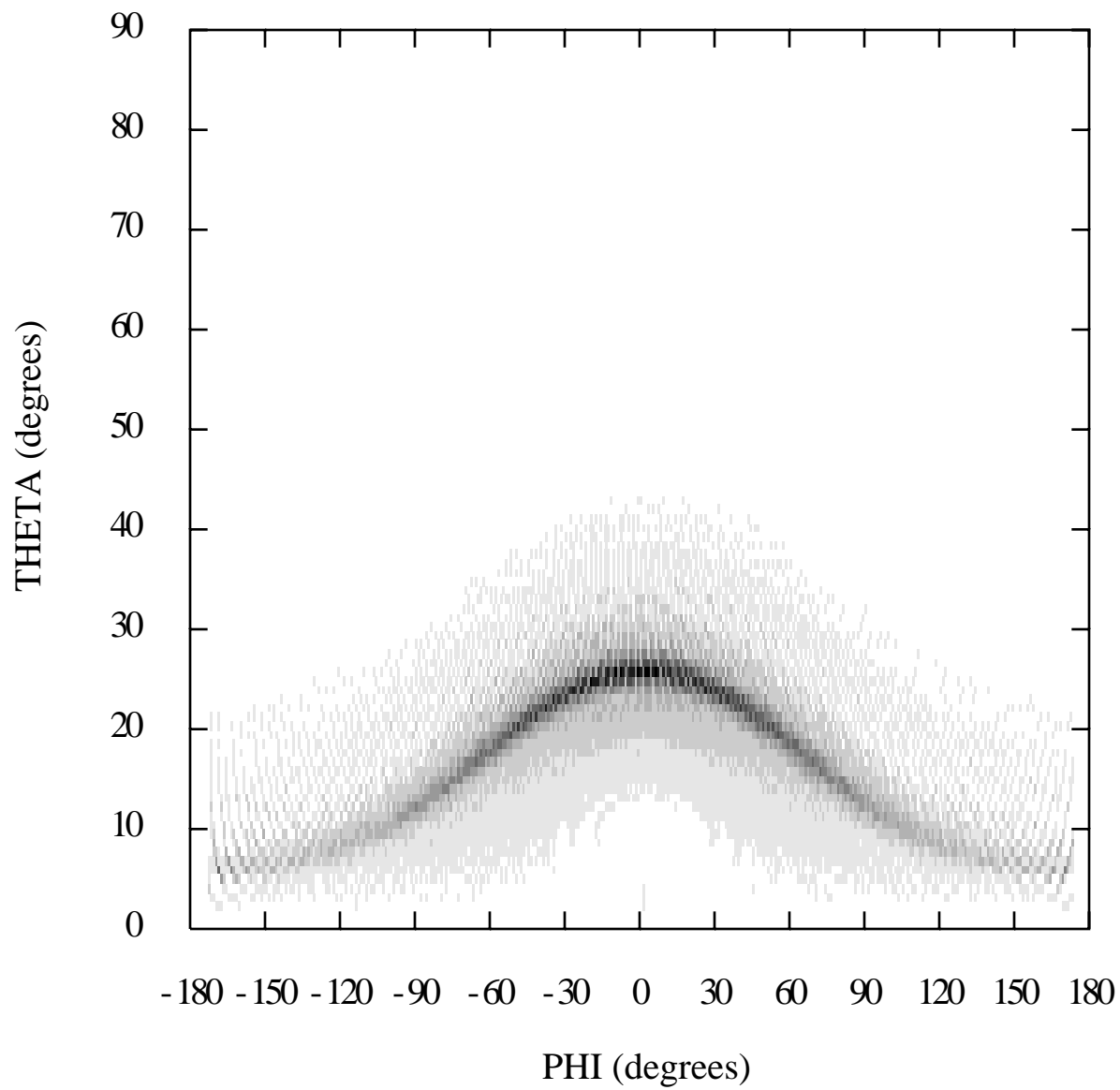
Lorentz Factor vs. Height



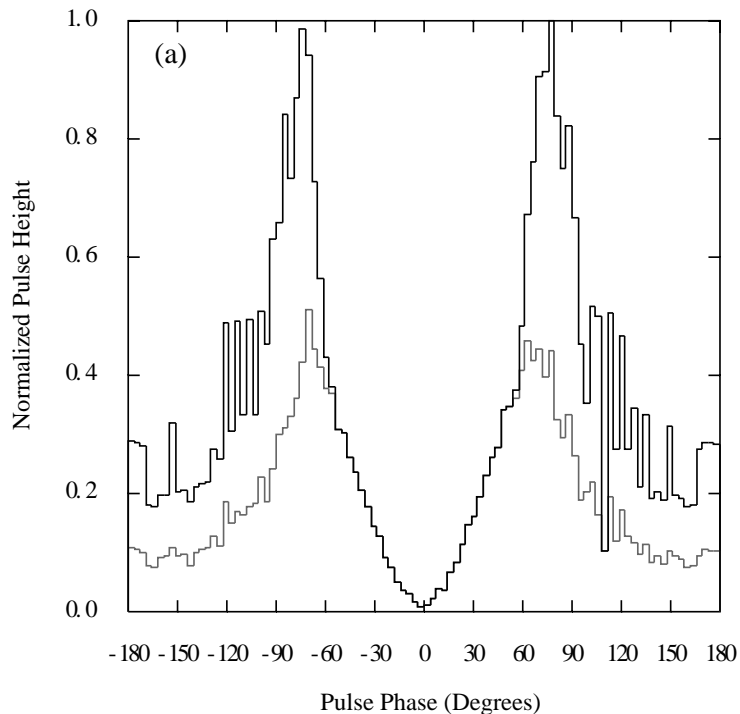
Multiplicity vs Height



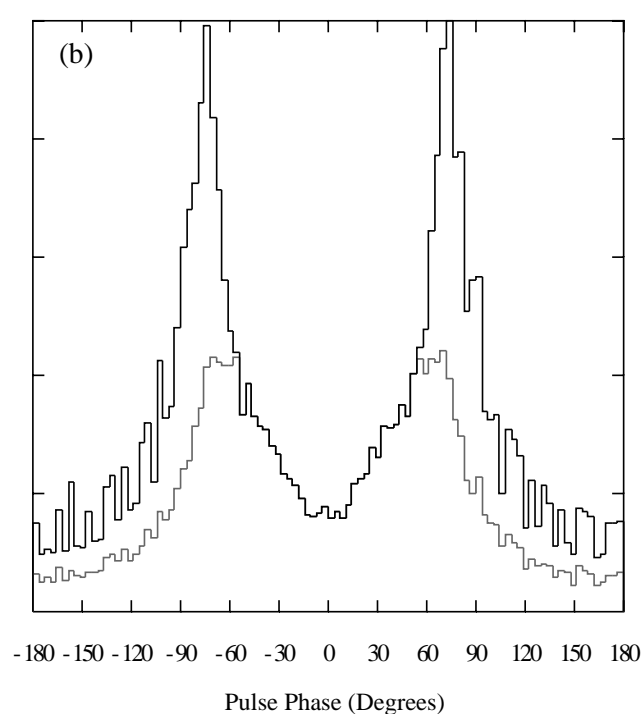
Cascade Gamma Radiation



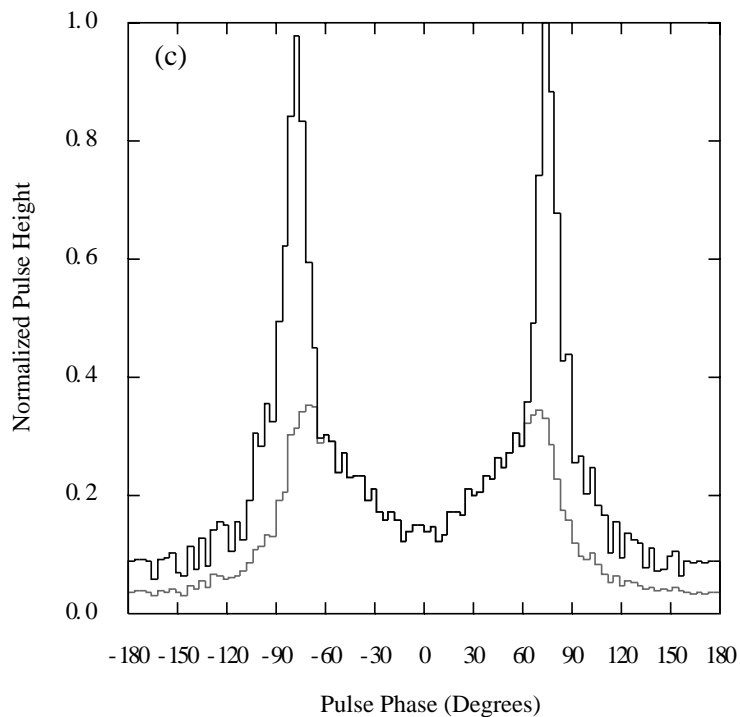
Vela Model A



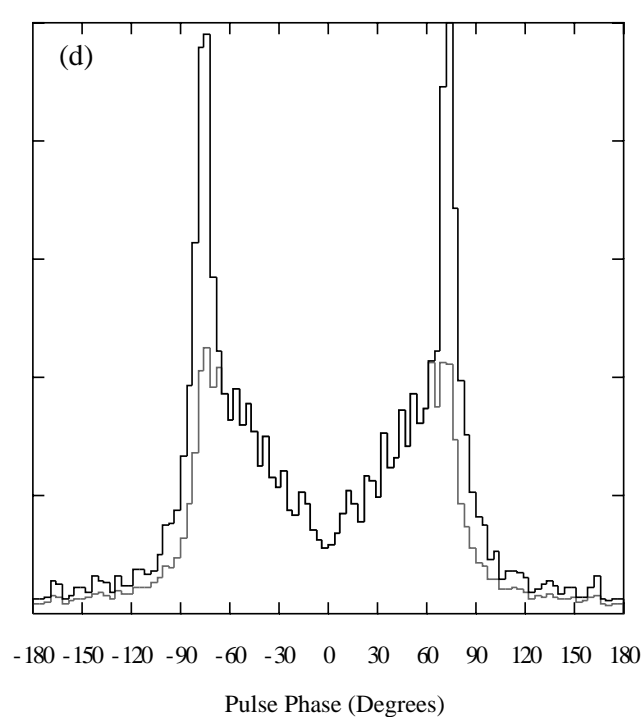
Vela Model B



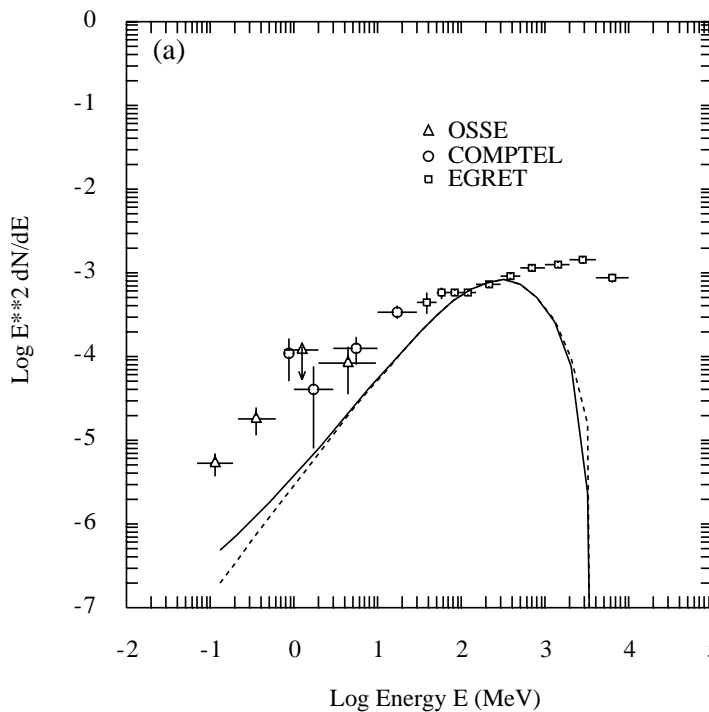
Vela Model C



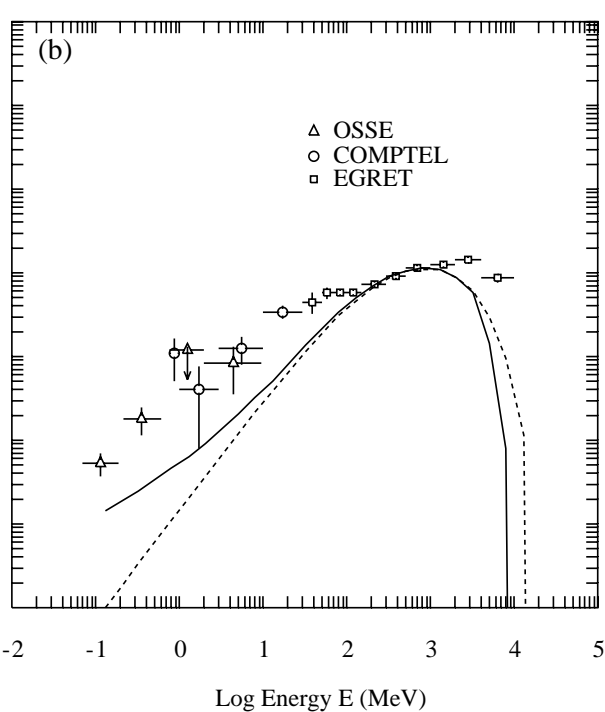
Vela Model D



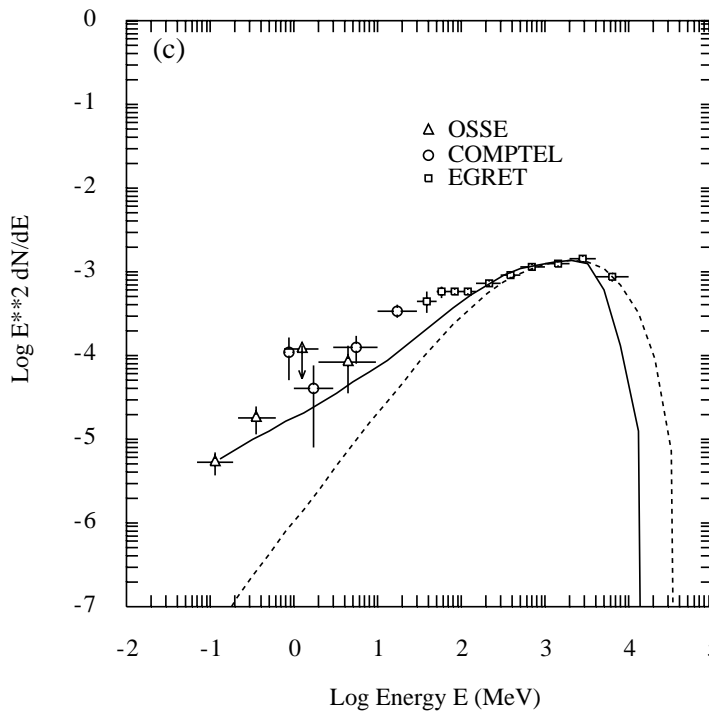
Phase-Averaged Spectrum: Vela Model A



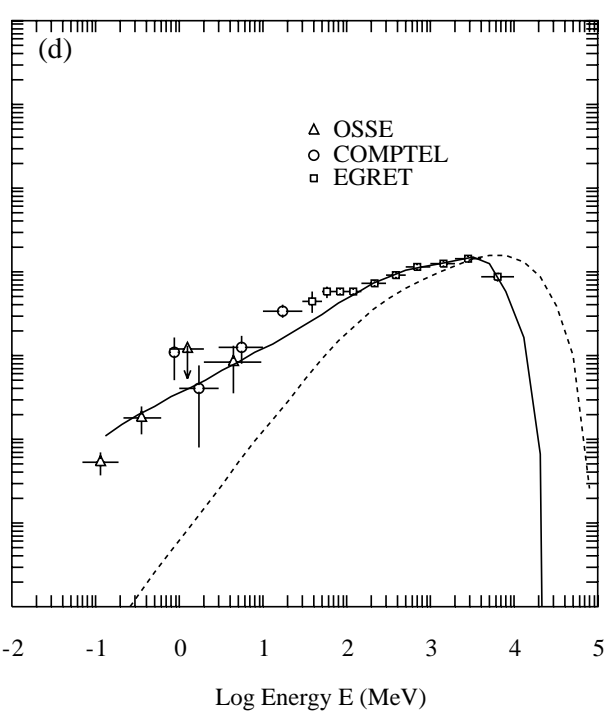
Phase-Averaged Spectrum: Vela Model B

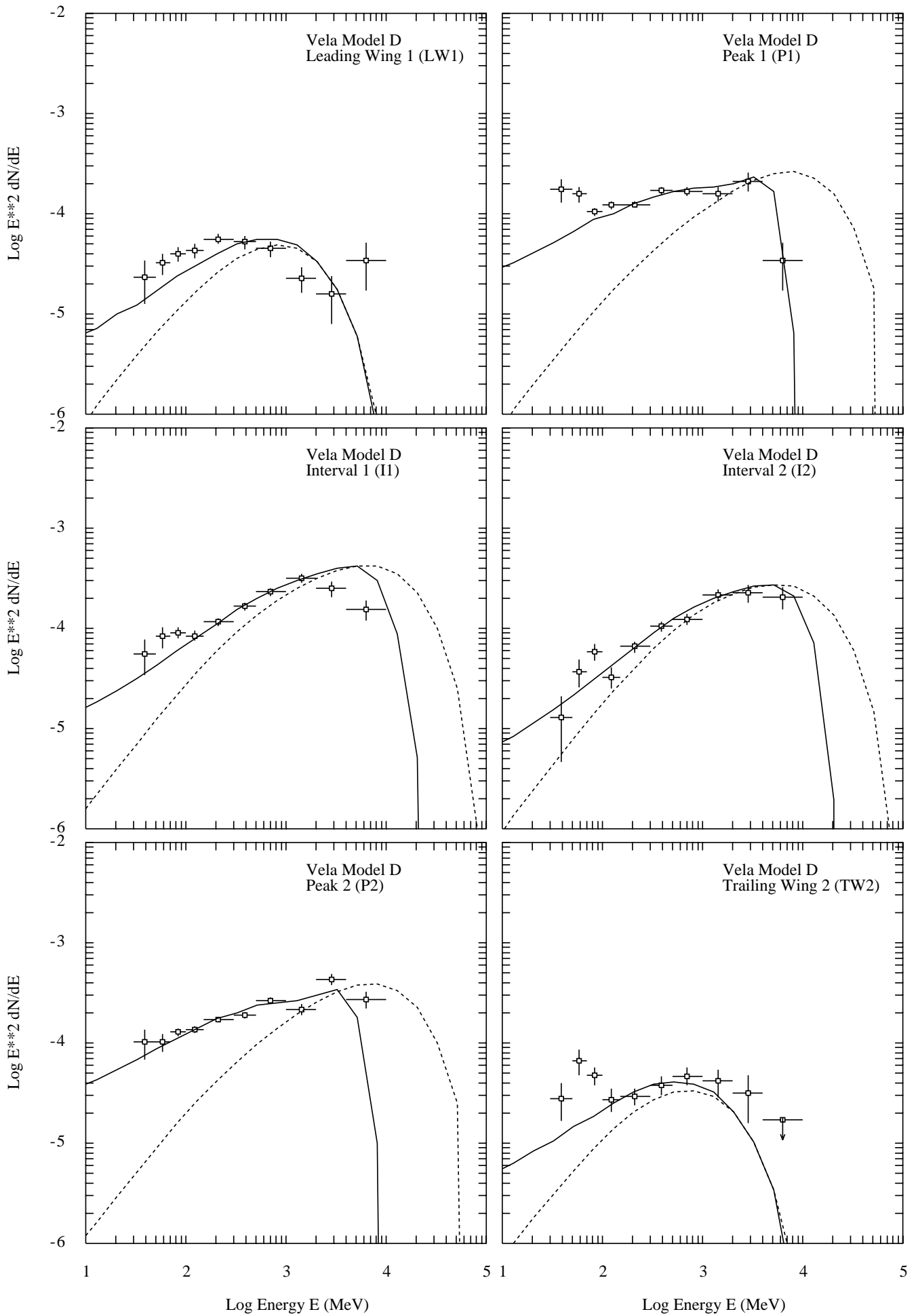


Phase-Averaged Spectrum: Vela Model C

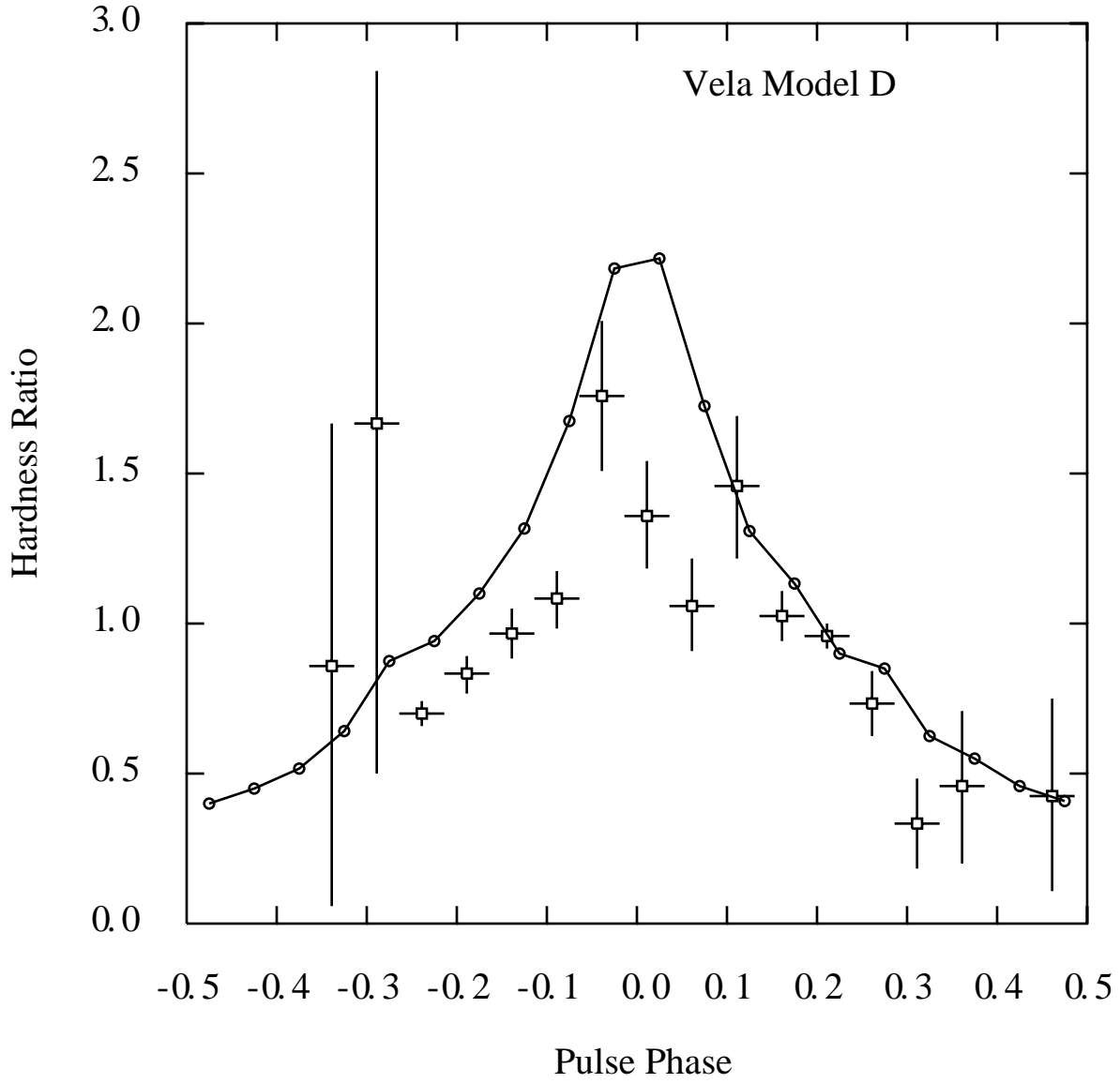


Phase-Averaged Spectrum: Vela Model D

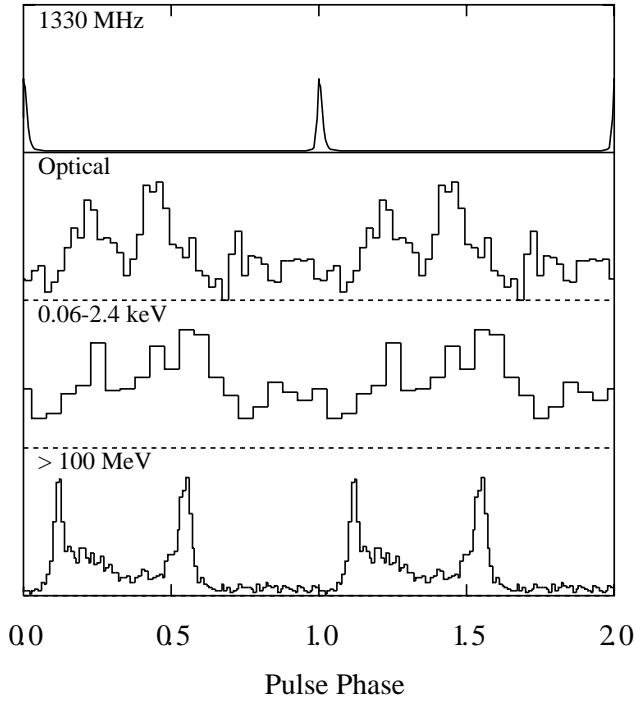




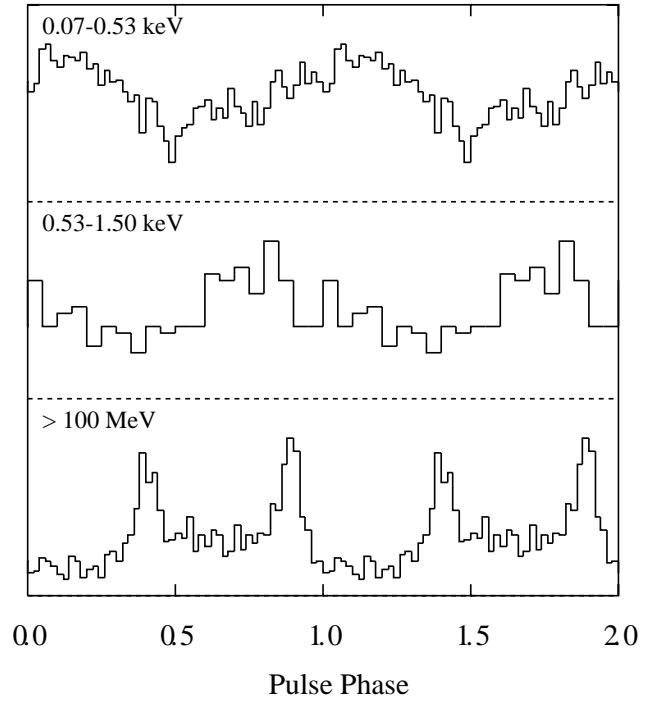
Hardness Ratio vs. Phase



(a) Vela



(b) Geminga



(c) PSR B1055-52

